Romanian Journal of Mechanics
Volume 4, Issue 2/2019, pp 47-64, ISSN 2537 - 5229, rjm.journals.srmta.ro

APPLICATIONS OF THE CHALCOGENIDE TERNARY THIN FILMS. A REVIEW

Nicoleta Nedelcu

Institute of Solid Mechanics, Romanian Academy

Corresponding author: Nicoleta NEDELCU, E-mail: nicoleta_dulgheru@yahoo.com

Abstract The chalcogenide ternary thin films chalcogenide glasses offer a new range of infrared transmitting materials to the designer and this review attempts to bring together the currently available data on these glasses. Information is presented on glass preparation, composition, softening temperature, thermal expansion, viscosity, chemical durability, mechanical properties, electrical properties, infrared transmission, refractive index and absorption coefficient, with particular emphasis on infrared transmission. Recent work has shown that impurity absorption bands have limited the infrared transmission of chalcogenide glasses.

Key words: Chalcogenides, infrared field, transparency, IR.

1. INTRODUCTION

In the last decades, the chalcogenide ternary thin films have attracted the attention of researchers from all over the world. The reasons are both scientific and applicative and have been catalyzed with each other over the years. Since the early 1900s, materials have been sought for various applications that are transparent in the infrared (IR) field. An important step in the identification and study of materials, which have an IR transparency of up to 7-8 μm, are the oxide materials [1, 2].

The combinations of the elements in group VI of the periodic table were studied to extend the transparency field in IR. The sulfur, selenium and tellurium compounds, with the generic name of chalcogenides, have occupied important places. The name *chalcogenide* comes from the Greek indicating that they occur in nature in copper ores (χαλκοζ - copper, γενναω - born and ειδοζ - type) [3]. Chalcogenides contain at least one chalcogen anion (e.g. S^{2-}) and an electropositive element (e.g. Cd^{2+}, Zn^{2+}). Often chalcogenides are mentioned as elements of the oxygen family but in this case, oxygen is treated separately from the other calcogens, being excluded even from the definition, due to its different chemical behavior.

The most important chalcogenides contain S, Se, Te (Fig.1). For example, sulfur-based materials are sought in most applications in the field of optoelectronic devices.

Selenium-based materials are most commonly used for imaging, biomedical applications, electrochemical sensors and solar cells, and tellurium materials are commonly used in memory devices and as infrared detectors [3-5].

The class of chalcogenides is represented by binary, ternary or quaternary combinations that are amorphous, crystalline or quasi-amorphous. Chalcogenides have special infrared properties, and the refractive index can be modified as needed. Chalcogenetide materials have imposed themselves as a distinct chapter in solids physics due to the photoinduced changes observed in the non-crystalline solid state [3].

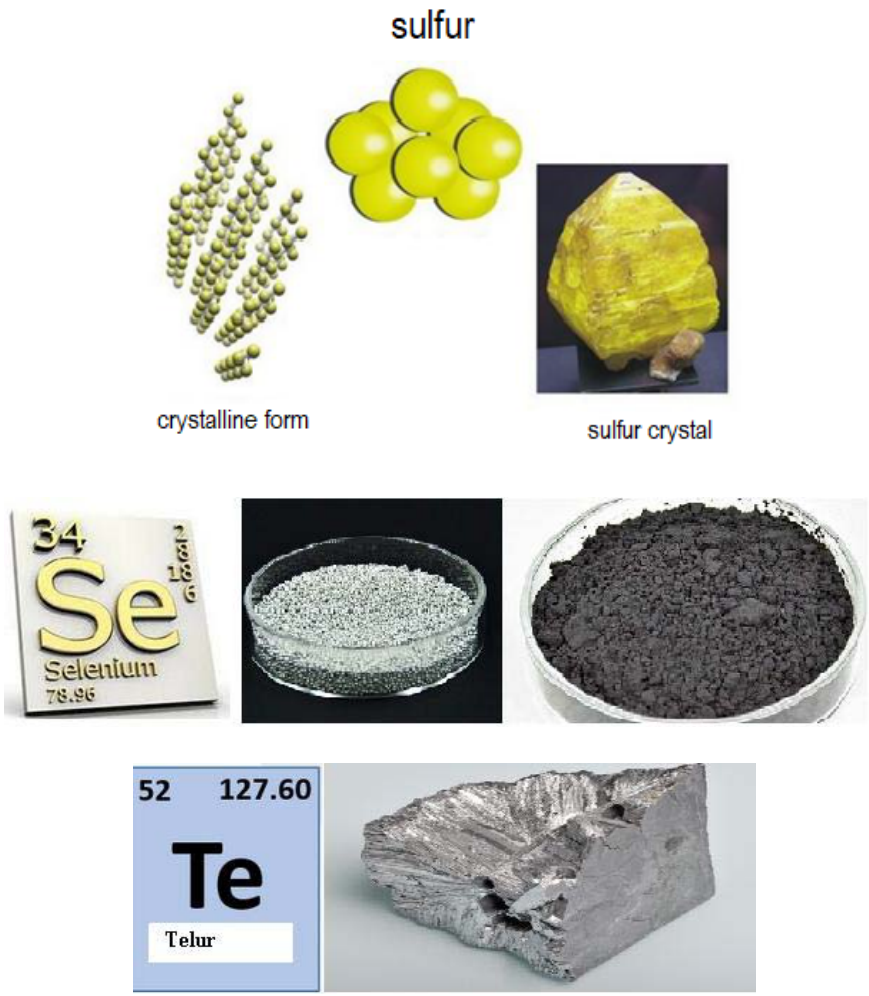

Fig.1. The most important calcogens [5].

The interest for non-crystalline chalcogenide materials has increased due to the presence of reversibility of some photoinduced phenomena, namely: the reversible change of the absorption coefficient or the refractive index [3-5].

In 1955, Kolomiets and Gorunova from the Ioffe Institute [6-7] showed that the semiconductor properties of chalcogenide materials alter their electro-physical and optical parameters under the action of an electric field, or by exposure to radiation. Reznik, Ohta and co-workers developed a selenium-based X-ray imaging system that is successfully applied in medical radiographs [8-9].

Tejaswini [10,11] nd colleagues developed sensors based on Ge-Sb-Se, using the conventional method of 99.999 at% purity elements by thermal evaporation in vacuo at evaporation temperature of 200 °C on different media. The sensors have been designed in such a way as to present good transparency over a wide range in IR.

The most commonly used supports in the literature with good transparency up to 5μm are quartz bottles. Subsequently, for the extension of the domain, the silicon and germanium substrates were studied, thus obtaining films with a transparency of up to 12μm. The films presented in the thesis were prepared on quartz substrate, by the same method, the evaporation of the material being done at room temperature.

The durability properties of the obtained films were tested according to US Military Standards (MIL-STD) [12]. These standards include specific requirements for various optical coatings.

Because films are thin [μm] porous and are often deposited on surfaces that are not chemically related, they are vulnerable to degradation from chemical, thermal and mechanical interactions. The tests revealed the stability of the films, thus demonstrating that durable thin layers of GeAs (Sb) STe can be obtained on quartz support at room temperature.

2. CLASSIFICATION OF CHALCOGENIC MATERIALS

The chalcogenides can be grouped into: *monochalcogenides, dichalcogenides, trichalcogenides,* and *tetrachalcogenides*. The monochalcogenides have the formula ME, where M notes a transition metal and E = S, Se,Te. These materials crystallize according to the corresponding forms of zinc sulphide. In the structure of the zinc sulfide mixture, the sulfur atoms are in a cubic symmetry, and the Zn^{2+} ions occupy half of the interstitial spaces. The main structure for monochalcogenides is the wűrtzit type structure in which the atomic environments are similar (tetrahedral), but the symmetry of the crystal is hexagonal [13-14] (Fig.2).

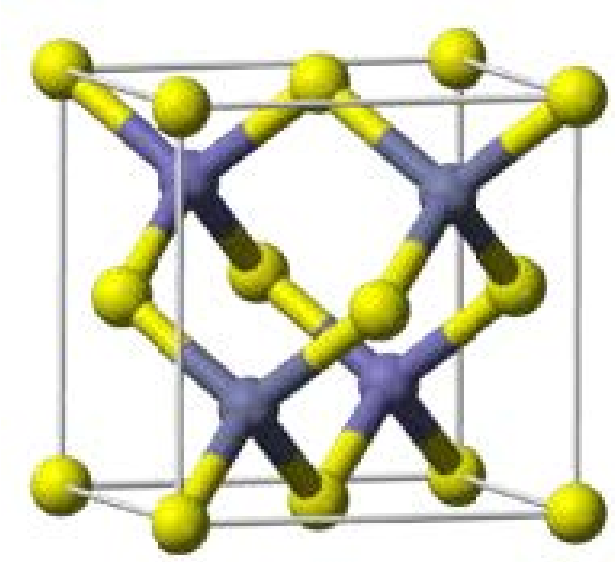

Fig. 2. Structure of the zinc sulphide [14].

Dichalcogenides have the formula ME_2, where M is a transition metal and E is S, Se, Te [14-16]. As usual, the most important members are sulfides.

These materials are solid, and have semiconductor properties. Regarding electronic structures, these compounds are usually seen as derivatives of M^{4+}, where $M^{4+} = Ti^{4+}$ (configuration d^0), V^{4+} (configuration d^1), Mo^{4+} (configuration d^2).

Titanium disulfide is the most well-known dichalchogenic material, is an inorganic compound of the formula TiS_2, a golden yellow solid with high electrical conductivity, and ME_2 stoichiometry used as cathodic material in rechargeable batteries. Molybdenum disulfide, has been the subject of many thousands of publications, is the main molybdenum ore and is called molybdenite, being used as a solid lubricant and catalyst for hydrodesulfurization.

In Fig.3 the strong bond between metal and chalcogenide ligands contributes to their intercalation with alkali metals, the intercalation process being accompanied by the charge transfer [15-17]. Dishelenides and even dithelurides are also known in this class, for example: $TiSe_2$, $MoSe_2$ (Fig. 3) and WSe_2 [16].

Trichalcogenides are usually described as M^{4+} $(E2^{2-})$ (E^{2-}) (where E = S, Se, Te) [17]. A well-known example is niobium triselenide or complex combinations of ternary GeSbSe films.

Formula VS_4, is an example of a metal tetrachalcogenide, crystallographic analysis shows that the material can be considered a bis (persulfide), ie V^{4+}, $(S2^{2-})_2$. Typically, the stoichiometry of these materials presents the classical valence values, an example being the combinations of the quaternary GeSb (As) STe films [18].

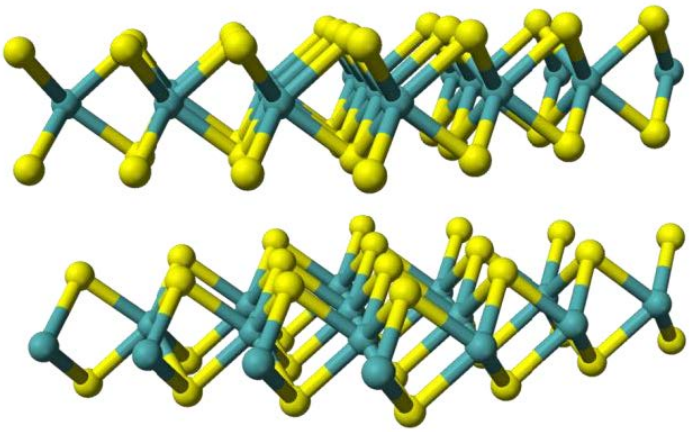

Fig.3. $MoSe_2$, the most common dichalcogenide adopting a branched structure [15].

3. PROPERTIES OF CHALCOGENIDE TERNARY THIN FILMS

Chalcogenide materials can be obtained by a wide range of methods, some of them being used to withstand mechanical wear or chemical corrosion. In the case of obtaining the thin layers it is very important that their thickness is uniform in order to be able to control very well the composition of the layers from the deposition phase. Also, the microstructure of the layers they are obtained is very important, because it is closely related to their physical properties [19].

These materials are used in many fields of science and technology. The most spectacular applications of chalcogenides are in microelectronics and optoelectronics, which is why new methods have been developed for obtaining high quality chalcogenide films for different purposes and applications [20].

Their physical properties are determined by a series of parameters such as:

- properties of the source materials in massive state used for the preparation of layers;
- properties of the substrate: roughness, crystalline ordering, amount of impurities on the surface (contamination) [21, 22].

Chalcogenides can be prepared by hydrothermal method [23], method of thermal evaporation in vacuum [24], thermal evaporation by laser ablation [25, 26] and radio frequency field scattering (RF Sputtering) [26, 27].

In the following, we present the properties of glassy systems $Ge_xSb_{20-x}Te_{80}$ alloys with composition $x = 15$, 17 and 19 at.%, are synthesized from elements with 5N purity (Ge, Sb, Te) by the conventional melt-quenching method [28-31]. The mixture of the elements with proper weight percent was put in a quartz ampoule which was evacuated down to 10^{-3} Pa. The ampoules were loaded in a rotary furnace and were heated up to 950°C.

For obtaining homogeneous melting, the glassy mixture was kept continuously at this temperature for 12h by rotating the furnace. After ending the process, the ampoules were pulled out, and the melts were rapidly cooled down in ice water.

Parts of the synthesized glasses were served as parent material for deposition on quartz substrate using a resistive crucible of 0.1mm molybdenum sheet from having the shape and size

from the UMICORE catalog. Degassing took place at 10^{-1} Pa, for 12 minutes in the atmosphere of N_2 and during this time, the dome is rotating (about 10 rot/min).

This process removes the impurities on the walls from the vacuum deposition installation and on the bulk. At 4×10^{-3} Pa pressure, the heating resistance is coupled, ensuring a temperature of 300^0C in the evaporation chamber while rotating the dome at the speed rotation of 10 rpm. Powder material was evaporated at least 400mA electric current.

Monitoring of the deposition control was done by TFCalc 3.5 software for approximate 6 minutes with a deposition rate of 3 nm/sec and showed 1300 nm thickness.

After evaporation, the samples were measured by VASE ellipsometer-Woolam. The ellipsometric's measurements were recorded in the spectral range UV-VIS-NIR. Fig. 4 shows the exeprimental Ψ and Δspectra with the best-fit obtained according to the wavelength.

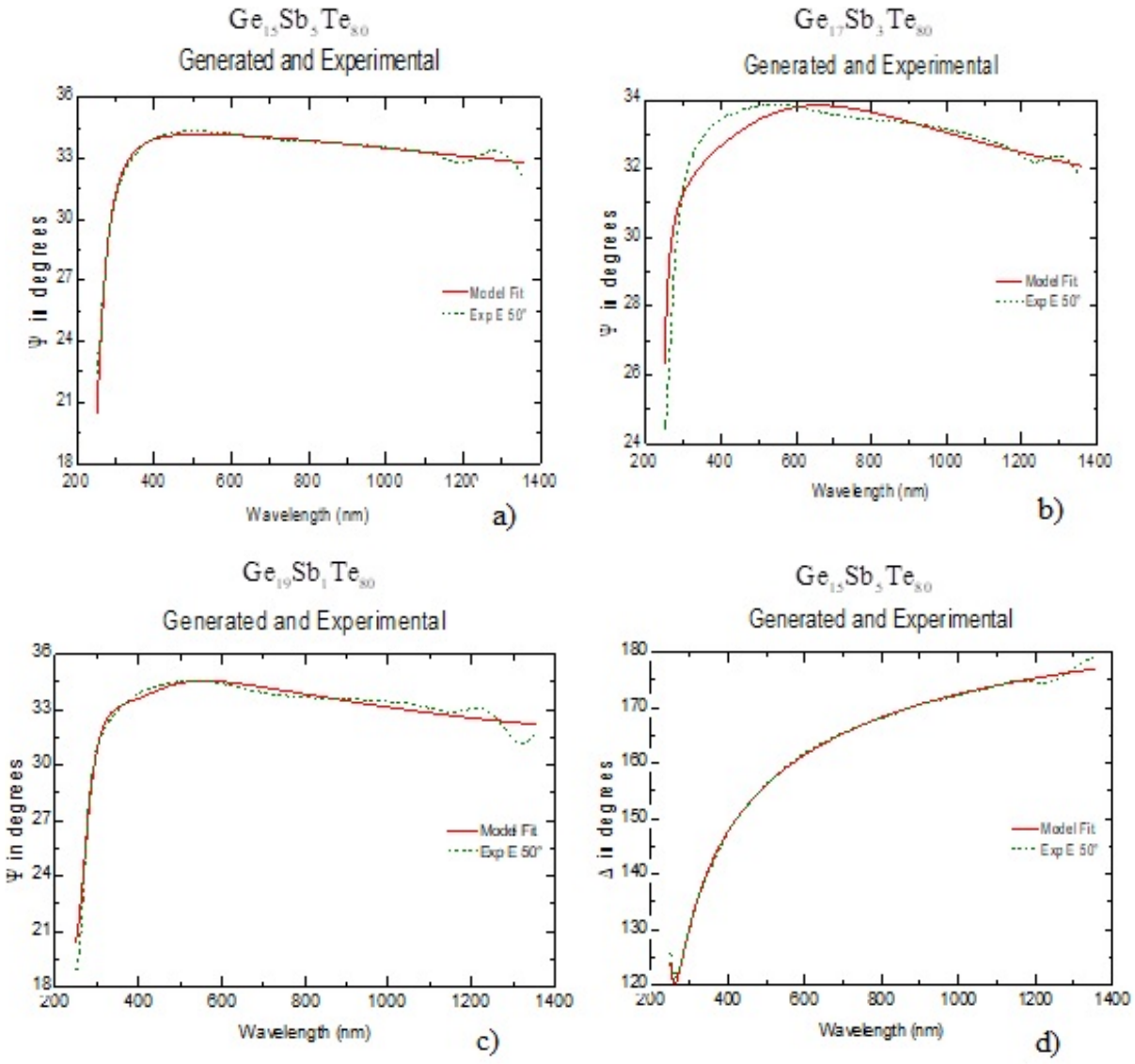

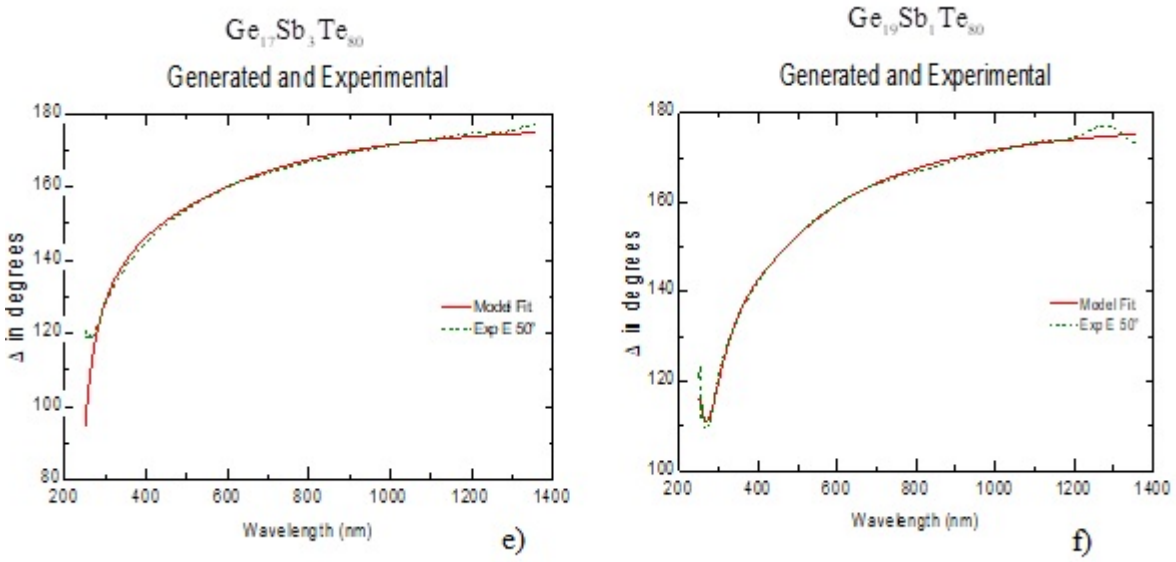

Fig. 4. a), b), c) The exeprimental Ψ and d), e), f) Δ spectra with the best fit obtained to $Ge_xSb_{20-x}Te_{80}$ alloys with composition $x = 15$, 17 and 19 at.%.

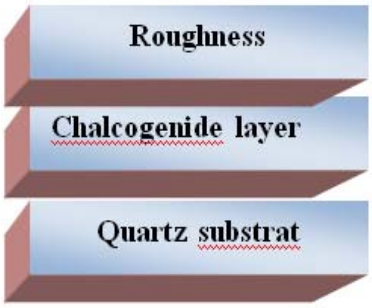

Fig. 5. The model layers on the quartz substrate.

Having the experimental data, the optical constants (*n* and *k*), are determined. The model contains 2 layers on the quartz substrate (Fig. 5), roughness layer / chalcogenic layer / substrate.

The chalcogenide layer was simulated by the General Oscillator method involving the Gauss and Lorentz oscillators.

The roughness layer, which is considered a mixture of 50% material (film) and 50% voids (air), was modeled with the Bruggemann's effective medium approximation (B-EMA). The optical constants (*n* and *k*) according to wavelength are presents in Fig.6.

According to the Fig 7 the optical constants decreases with the increase the Ge content. Fig. 8 shows the variation of the absorbtion coefficient $\alpha(\lambda)$ with respect to wavelength for $Ge_xSb_{40-x}Se_{60}$ alloys with composition $x = 12$, 25 and 30 at. %. The quantity $\alpha(\lambda)$ is given by

$$\alpha(\lambda) = \frac{4\pi k(\lambda)}{\lambda}. \tag{1}$$

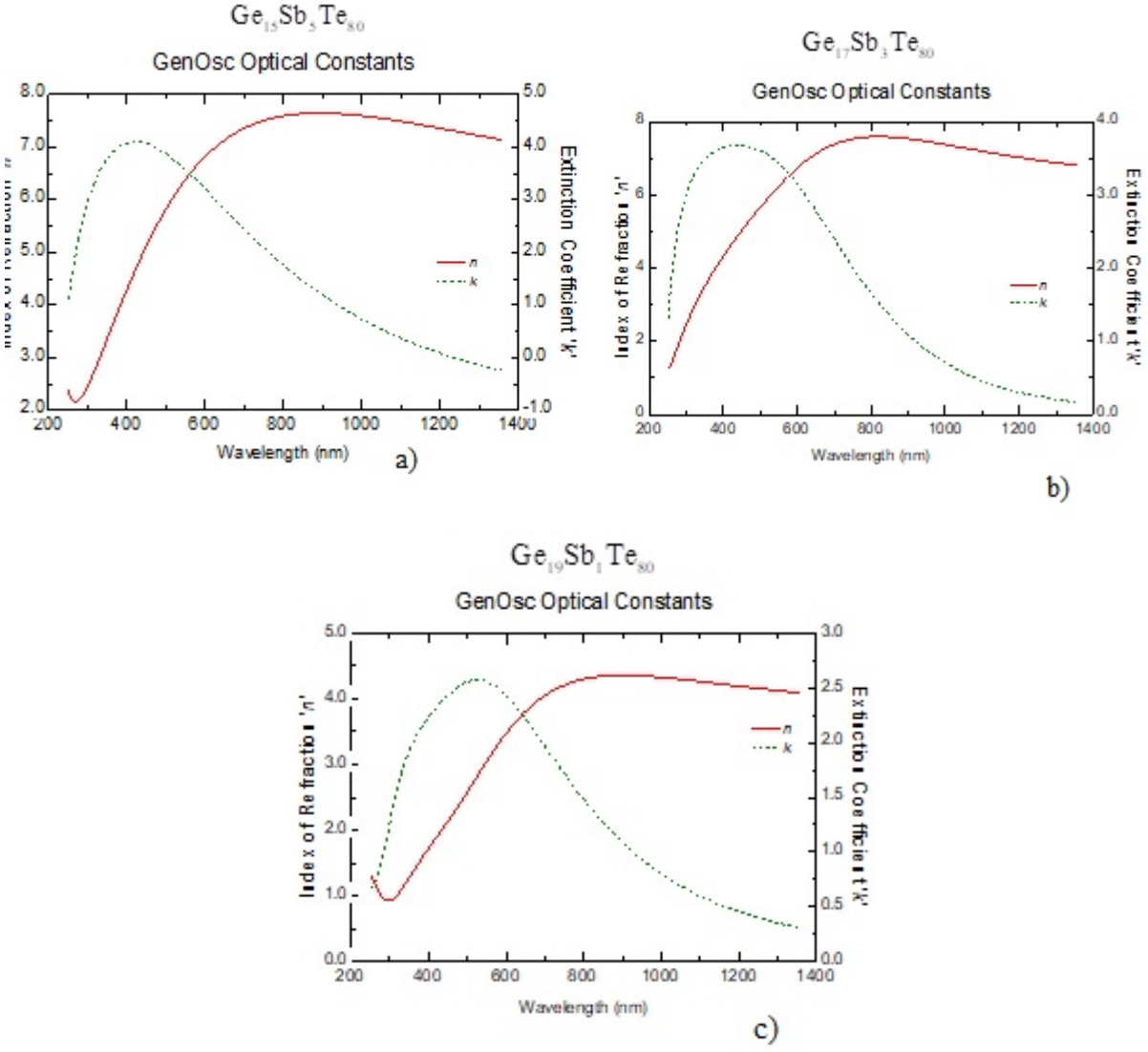

Fig. 6. The optical constants (*n* and *k*) for a) $Ge_{15}Sb_5Te_{80}$, b) $Ge_{17}Sb_3Te_{80}$, c) $Ge_{19}Sb_1Te_{80}$.

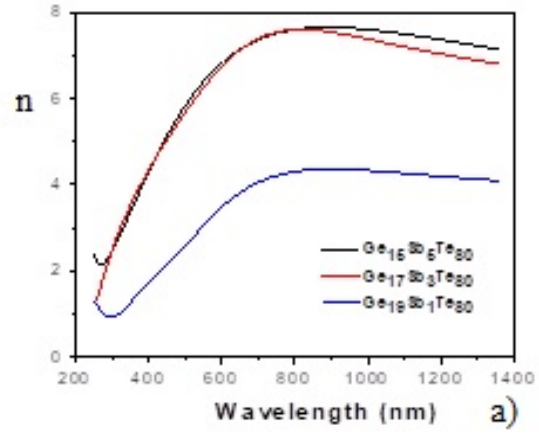

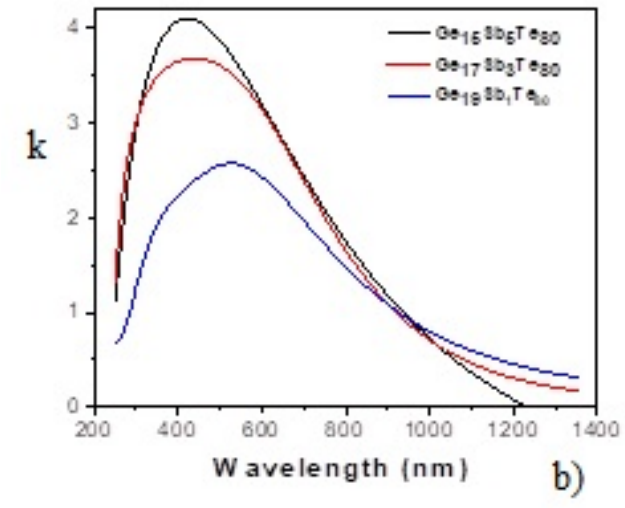

Fig. 7. Optical constants n (a) and k (b) for $Ge_xSb_{20-x}Te_{80}$ alloys with composition $x = 15$, 17 and 19 at.%.

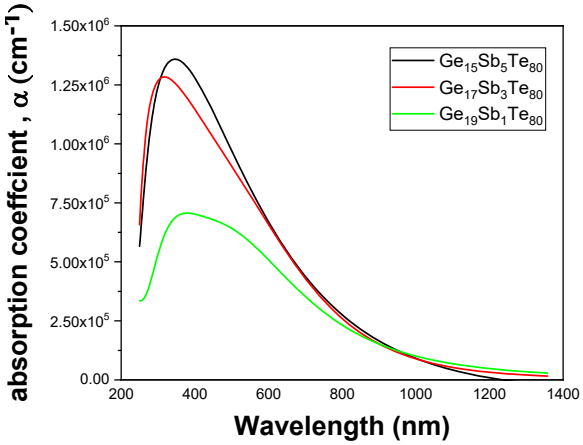

Fig. 8. Variation of the absorbtion coefficient $\alpha(\lambda)$ with respect to wavelength for $Ge_xSb_{40-x}Se_{60}$ alloys with composition $x = 12$, 25 and 30 at. %.

Chalcogenides are characterized by electrical and optical band gaps of 1-3 eV and then they are regarded as amorphous semiconductors. Gap decreases in the sequence of S, Se and Te, reflect an enhanced metallic character. The overall property of chalcogenides is shown in Fig. 9.

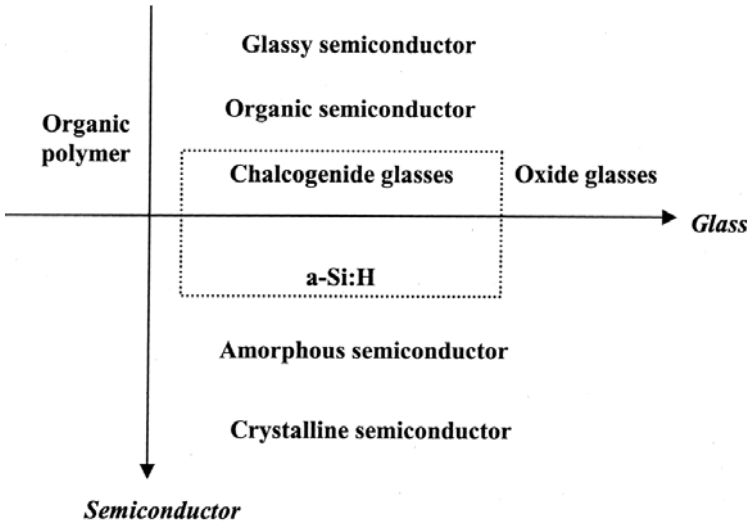

Fig.9. Characterization of chalcogenides and semiconductors in comparison with other materials [32].

4. APPLICATIONS OF CHALCOGENIDE THIN FILMS

Principal applications of chalcogenide thin films can be classified as: laser power delivery, chemical sensing and near-field microscopy.

The CO and CO_2 lasers transmit waves through fibers of chalcogenide thin films, operating at 5.4 μm and 10.6 μm, respectively. These lasers are used for industrial welding and cutting. For small core diameter smaller than 200 m, the fibers have a tolerance to power densities of 125 kW/cm^2 at 5.4 μm and 54 kW/cm^2 at 10.6 μm without damage. Fig. 9 shows (a) the pulsed high energy laser transmission in the 2-5 μm region, (b) CO laser transmission, and (c) CO_2 laser transmission [2].

Delivery of energy by the medical free-electron laser (MFEL) is based on the chalcogenide fibers, operating between 2 and 10 μm [28]. The MFEL emits more than 10 MW of power in a femtosecond pulse, this means an average power of greater than 10 Watts. In the surgery operations at 2.94 mm with the energy of 1-2 mJ, the chalcogenide fibers avoid the damage of the fibers as it happens for YAG laser with transmission through sulfide fiber.

Chemical sensing uses the property of chalcogenide films to vibrate in the infrared region. The chemical sensing is seen as the detection and identification of oil, freon, soap, paints, polymer curing reactions, glucose /water, benzene and derivatives in different media [2, 28-31]. Detection limits of 130 ppm of marine diesel fuel in sea sand and have been demonstrated using a 20-meter length of cable.

The chalcogenides are associated to strong vibrational modes of organic media; therefore, the broad infrared sensing can be used for biological, radiation and temperature sensors, detection of CO_2 and the micro-organisms and pollution in an environment [28-31].

Numerous devices work to detect aqueous, non-aqueous, perfumes and toxic liquids as well as solids in different media. Changes of oil in motor vehicles can be efficiently performed by using a fiber optic sensor to control the quality of the oil. So, the fiber optic sensor can control the degradation of oils, signaling the oil change [2].

Respiratory sensors are made for detecting carbon dioxide in the exhalation of a patient using the infrared absorption of carbon gases. This technique can be used during the process of Magnetic Resonance Imaging (MRI). Due to high electromagnetic field interference, it is difficult to measure biomedical factors such as respiration signals in the MRI environment. So, electromagnetic interference can be overcome by using a fiber optical sensor made up of dielectric material like

glass or plastic. Pulsed high energy laser transmission in the 2-5 μm region is presented in Fig.10a, the CO laser transmission in Fig.10b, while the CO_2 laser transmission ie presented in Fig.10c [2].

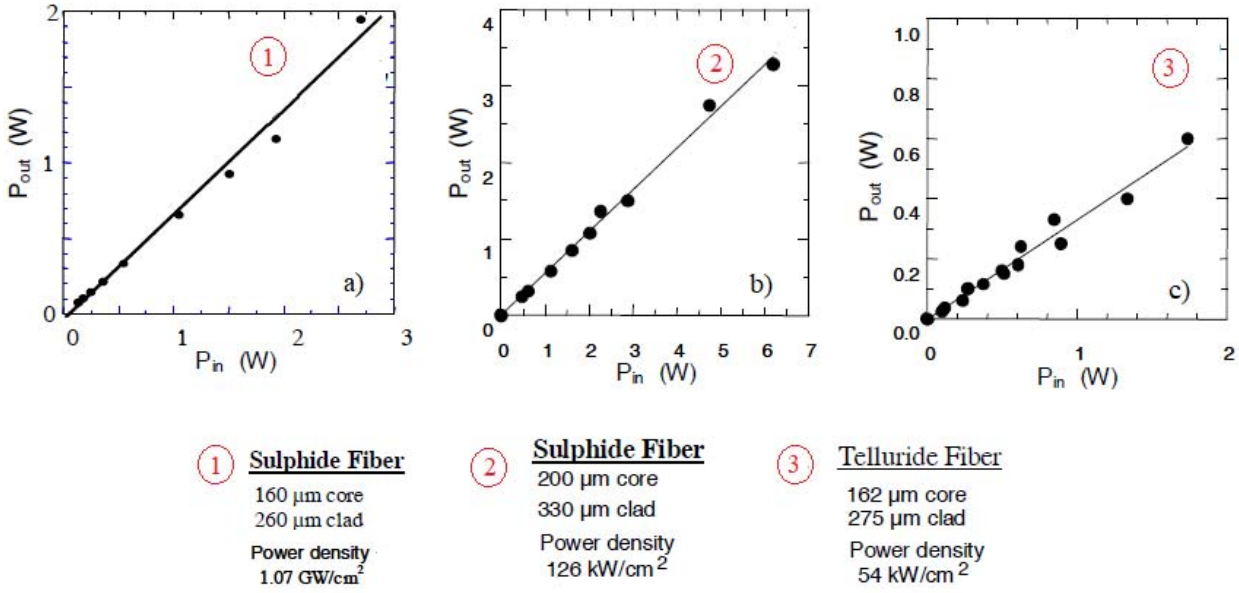

Fig. 10. (a) Pulsed high energy laser transmission in the 2-5 μm region, (b) CO laser transmission, and (c) CO_2 laser transmission [2].

Chalcogenide material of composition As_2S_3 are the best glasses used as the respiratory sensors, with the core (As_2S_3) diameter 0.50 mm, and thickness of the cladding (As-S) 0.015 mm. The refractive index of the core is 2.4. The ambient temperature range for surgery is from 7 to 127°C. The fundamental absorption line of carbon dioxide (CO_2) is 4.26 μm in the infrared range [28-31]. By using multimode chalcogenide fiber micro-tips with about 1 mm resolution, cca 20 nm topographic resolution and 200 nm spectral resolution for different samples such as polycrystalline diamond, pancreatic cells, biofilms and semiconductor samples are obtained. Fig.11 shows the optical spectra for a) polycrystalline diamond film at $\lambda = 3.5\mu m$ and b) the pancreatic cells at $\lambda = 6.1\mu m$. The optical spectra have a resolution of 25 nm and 200 nm, respectively [2]. The dark regions are due to absorption by the molecular vibrations.

Interatomic distances were taken from previous studies and from literature data based on similar or very close compositions. Several RMC simulations were performed by slightly modifying the interatomic distances at different pairs of atoms. Thus, the experimental S(Q) factors were compared with the data obtained from the RMC modeling. Almost 20 RMC configurations from each sample were obtained at intervals of more than 1,500,000 atoms accepted by the motions.

By combining with the RMC simulation of the X-ray and neutron diffraction methods, the parameters and possible chemical links existing in the structural units of the Ge-Sb-Se network were examined.

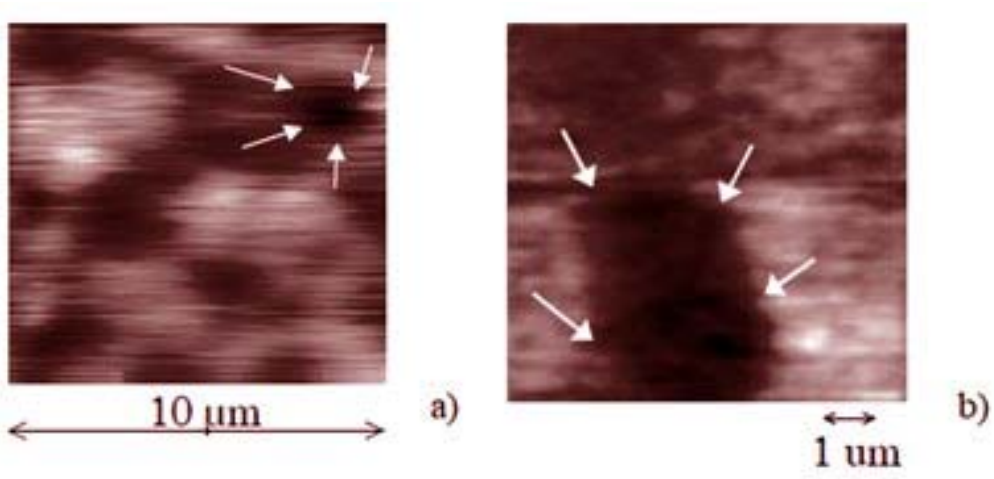

Fig.11. The optical spectra for a) polycrystalline diamond film at $\lambda = 3.5\mu m$ and b) the pancreatic cells at $\lambda = 6.1\mu m$ [2].

It was found that the Ge atom is coordinated by 4Se atoms and the Sb atom coordinated by 3Se atoms. ternary. To better see the chemical bond, in Fig.12 are shown Bravais cell models exemplified for ternary films of $Ge_{15}Sb_{25}Se_{60}$ and for $Ge_{35}Sb_5Se_{60}$ [28-31].

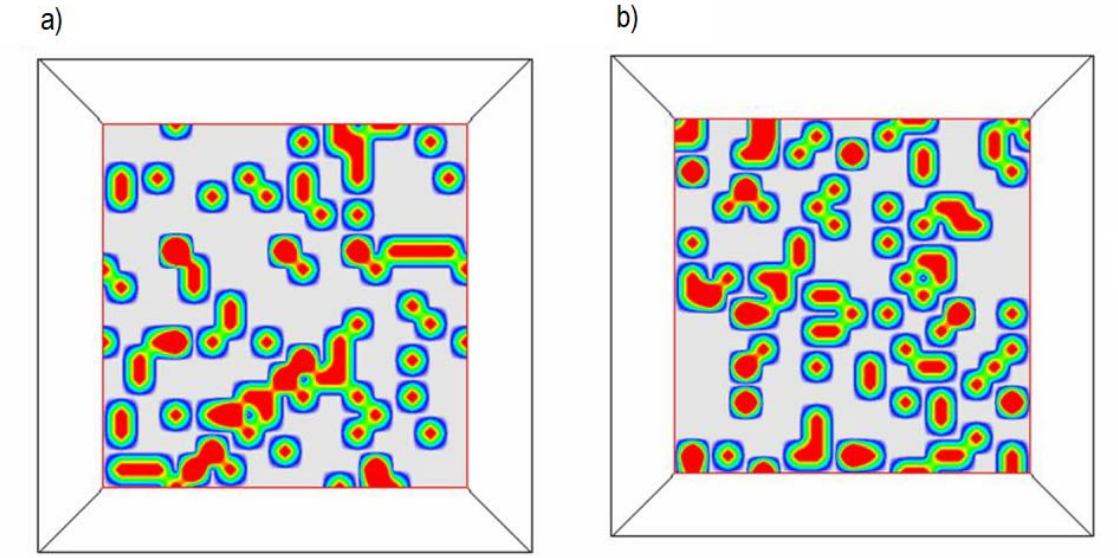

Fig.12. Atomic density for the plane $Ge_{15}Sb_{25}Se_{60}$ (a) and $Ge_{35}Sb_5Se_{60}$ (b) [28-31].

In Fig.12, for the given unit of cells, the atomic radii of Ge = 1.25 Å, Sb = 1.45 Å and Se = 1.15 Å were taken from the database, while the interatomic distances were taken from the last configuration of the particles in the RMC simulation, as follows:Ge-Se, r_{min} = 2.1 and r_{max} = 2.6 Å; Sb-Se, r_{min} = 2.3 and r_{max} = 2.8 Å. Color represents the atom type Ge-red, Sb-green and Se-blue [28]. A possible identification of the distribution functions of the pairs of Ge-Se and Sb-Se atoms can be done in a 3D simulation of a smaller configuration (200 atoms) for the ternary films of 40 $Ge_{15}Sb_{25}Se_{60}$ and for $Ge_{35}Sb_5Se_{60}$. The distribution functions of the pairs of atoms are evidence of the presence of short-distance bonds in the amorphous material. By increasing the Ge concentration, respectively decreasing the Sb concentration, the interatomic distances in the Ge-Se bonds increase from 2.37 Å to 2.40 Å, while for the links Sb-Se the opposite tendency is observed, because the atoms are randomly distributed, never all the atoms will be linked [28-31].

Even if the Ge/Sb ratio changes greatly, the base network units (Ge-tetrahedral and Sb-trigonal

units) are present in both compositions. Thus, at a certain value *x*, when the content of Ge increases, the cross-linking of the Ge atoms takes place in the chains of the Ge-Se bond (Fig.12b), which leads to a structural rearrangement in films, so that the films pass through a topological phase transition.

With relation to the Atomic Force Microscopy imaging of chalcogenides, the AFM investigations of the $Ge_xSb_{40-x}Se_{60}$ films supported the optical and structural observations and showed a threshold-like behavior in the compositional dependences of the surface morphology parameters.

The topographic AFM images for the deposited films reveal the fine granular structure of the Ge-Sb-Se glasses. The 2D AFM surface images of the $Ge_xSb_{40-x}Se_{60}$ films, taken from a 1μm×1μm scanned surface area give information on the surface is covered with nanometric grains, whose diameter is in the range of (16-22) nm.

Depending on the composition, some particularities could be noticed regarding the spatial distribution of the constituting grains [28].

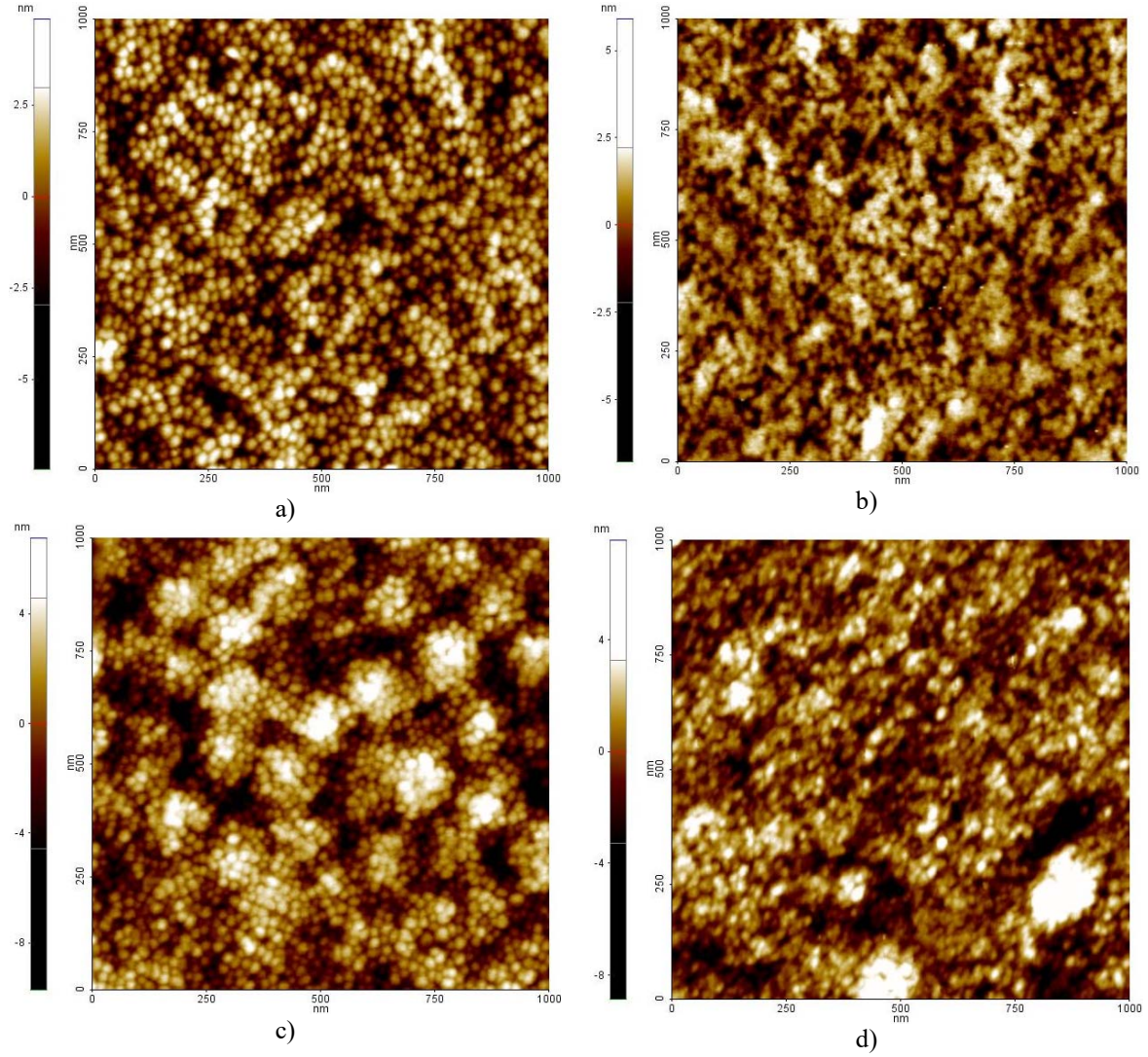

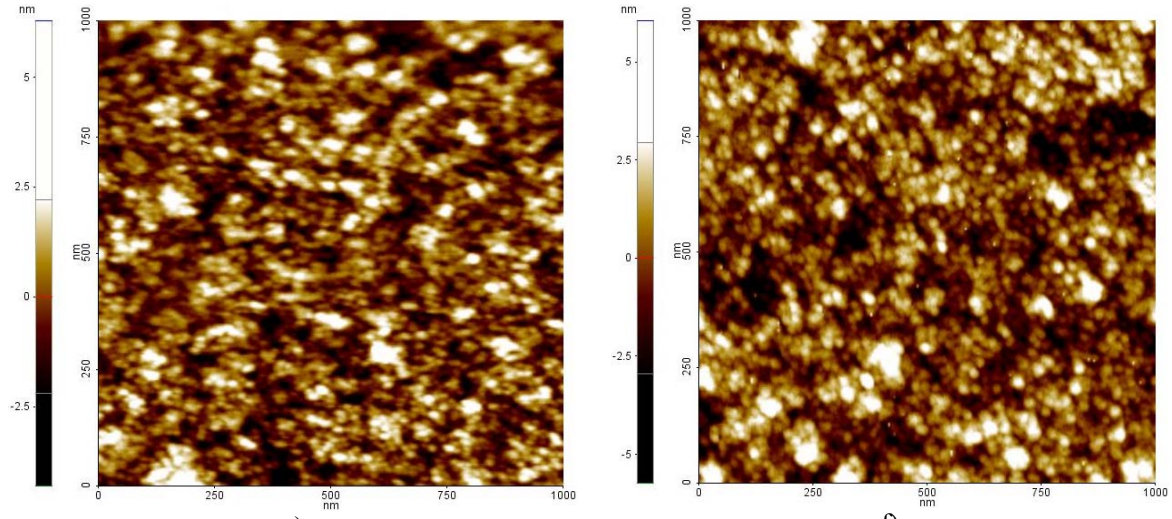

e) f)

Fig. 13. 2D AFM topographical image of the $Ge_xSb_{40-x}Se_{60}$ films surface taken at 1μm ×1 μm scan: x =15 at.% (a); x =20 at.% (b); x=25 at.% (c); x =27 at.% (d); x =32 at.% (e) and x =35 at.% (f) [28-31].

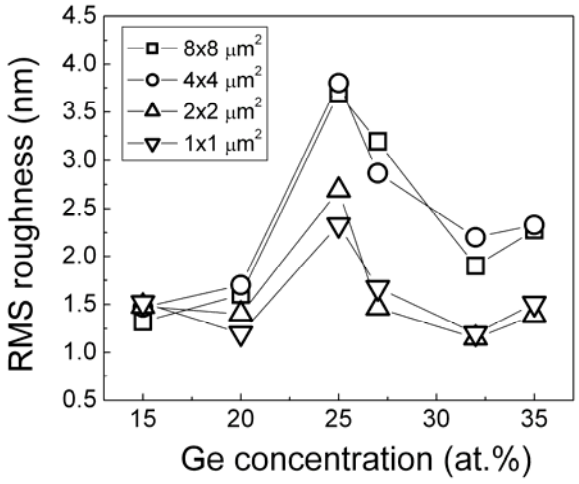

Fig. 14. RMS roughness dependence on the Ge content in the chalcogenide films at different scanning scales as indicated in the legend [28-31].

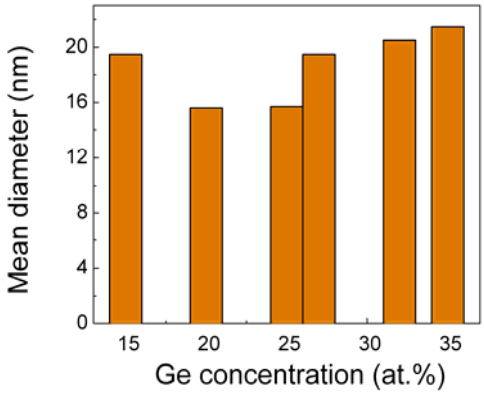

Fig. 15. Mean diameter size of particles coming up to the $Ge_xSb_{40-x}Se_{60}$ film surface [28-31].

By increasing the Ge content to 25 at. % (Fig.13 a,b,c) the surface particles tend to create cauliflower-like patterns, thus increasing the surface roughness due to their corrugation, created by the bunching of the grains in form of cauliflowers. Further increase of the Ge content leads to slightly disordered surfaces and decreased roughness values.

This is well seen in Fig. 14, where the root mean square (RMS) roughness values are obtained from different scanning areas of (1×1), (2×2), (4×4) and (8×8) μm^2, as indicated in the legend. A maximum in the compositional dependence is observed at x =25 at.% which corresponds to an average coordination number of Z = 2.65.

In Fig. 15 the mean diameter size of particles coming up to the surface is given. By increasing the Ge content from 15 at.% (d~ 20 nm) to 20 at.%, the diameter of the surface particles become even smaller (d~16 nm), but some valleys (visible as irregular black dots or black islands) are formed, which increase the surface porosity.

Further increase of the Ge leads to enlargement of the surface particles. At Ge content in the range of (27-35) at. %, the chalcogenide films exhibit similar morphologies and surfaces that are covered with particles of 19-22 nm in diameter).

The particles are randomly gathered creating hills (visible as white areas) and valleys (visible as dark areas/parcels).

In order to quantitatively evaluate the film surface texture, the AFM images were further analysed with Scanning Probe Image Processor software package (SPIP™ v4.6.0.0). The surface amplitude parameters, namely the peak-to-valley height S_y, average surface roughness S_a and root mean square (RMS) roughness S_q quantitatively describe how rough the surface is.

By examining the degree of surface skewness S_{sk} and surface kurtosis S_{ku} we receive quantitative information about the surface morphology (texture).

These quantities are summarized in Table 1.

In general, the $Ge_xSb_{40-x}Se_{60}$ films exhibit smooth surfaces with RMS roughness values in the range of (1.1-2.3) nm at the scale of (1×1) μm^2.

Even at larger scales, of (4×4) or (8×8) μm^2, the roughness does not exceed 3.8 nm for the most corrugated surface. The peak-to-valley parameter S_y stands in line with the roughness behavior.

The kurtosis parameter, S_{ku}, which evaluates the randomness of profile heights, is ~3 for x =15 at. %, and could be described as having a Gaussian distribution of the surface features, while the increase of the kurtosis parameter over 3 is due to an increase weight of large and sharp peaks and valleys.

The surface skewness, S_{sk}, which is related to the asymmetry of the height distribution, is slightly positive for the films with Ge content of 15-25 at. % and switches to slightly negative values for the films with higher Ge content because of the increasing weight of the pores (valleys).

Table 1. Surface amplitude parameters for a 1×1 μm^2 scanned area of the $Ge_xSb_{40-x}Se_{60}$ films.

Film composition	S_y (nm)	S_a (nm)	S_q (nm)	S_{sk}	S_{ku}
$Ge_{15}Sb_{25}Se_{60}$	12.32	1.22	1.52	0.38	3.03
$Ge_{20}Sb_{20}Se_{60}$	12.68	0.90	1.13	0.49	3.47
$Ge_{25}Sb_{15}Se_{60}$	16.45	1.90	2.33	0.18	2.76
$Ge_{27}Sb_{13}Se_{60}$	16.42	1.28	1.67	-0.12	4.19
$Ge_{32}Sb_{8}Se_{60}$	11.19	0.94	1.20	-0.21	3.36
$Ge_{35}Sb_{5}Se_{60}$	11.79	1.20	1.51	-0.14	3.15

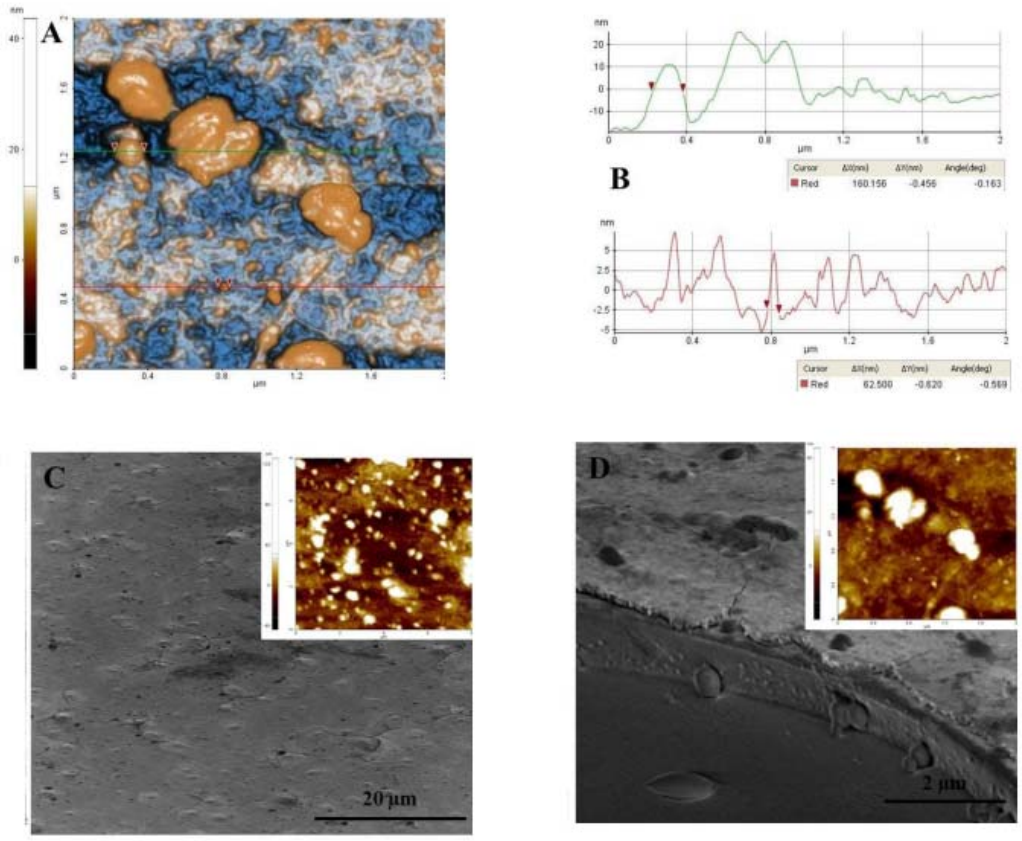

Fig.16. *Surface morphology for $Ge_{27}Sb_{13}S_{50}Te_{10}$ before performing the quality standard tests investigated by AFM and SEM.*

At larger scales, e.g. (4×4) and (8×8) μm^2, the amplitude parameters, follow the RMS roughness shape, exhibiting highest values at 25 at. % Ge content. Nevertheless, the spatial arrangements of the surface particles create areas with aspect of hills (merged grains) and valleys (pits/pores).

The ellipsometric analysis of the effect of *quality tests* showed that the thickness of the films decreases slightly after the quality tests, while the roughness the surface is strongly affected by tests.

A more visible effect can be seen on samples with a high Sb content. In this case, the surface roughness increases and the surface roughness decreases. The refractive indices exhibit different behavior function on the composition.

Thus, the refractive indices of the films with a high As content are not influenced by the tests, nor those with high content of Ge, their values being about 2.8 for all series. The refractive index for high Sb-content is increasing. The surface morphology for $Ge_{27}Sb_{13}S_{50}Te_{10}$ before performing the quality standard tests are investigated by AFM and SEM.

Fig.16 shows the surface morphology for $Ge_{27}As_{13}S_{50}Te_{10}$ before and after the quality standard tests investigated with AFM and SEM.

CONCLUSIONS

The chalcogenide materials have been synthesized from elements with 99.999% purity by the vacuum evaporation method at room temperature deposited on the quartz substrates. The structural properties of ternary films were investigated by XRD and ND coupled with simulation procedure Reverse Monte Carlo (RMC). It has been found that the addition of the Sb atom initially does not

modify the Ge-tetrahedral basic structural units, but the Sb concentration increases or the well-defined Sb-pyramid units are formed.

The optical properties of the ternary and quaternary systems were analyzed by ellipsometry in the UV-VIS-NIR domain. The ellipsometric IR study was performed to determine the information on chemical bonds. Thus, the vibration band positions have been established and the related chemical bonds have been identified, confirming that the evaporated films do not contain water.

However, defects related to the appearance of oxygen bonds (Ge-O and Te-O) were present in films, most likely due to surface oxidation over time. AFM images for all chalcogenic systems have revealed a completely coated surface with evenly distributed granules and having a particular structure depending on the film composition.

Morphological analyzes of samples before and after quality tests revealed the stability of quaternary films containing As, while quaternary films containing Sb are less resistant. Moreover, the quality tests have led to better relief surfaces due to the removal of a superficial layer (including surface contaminants).

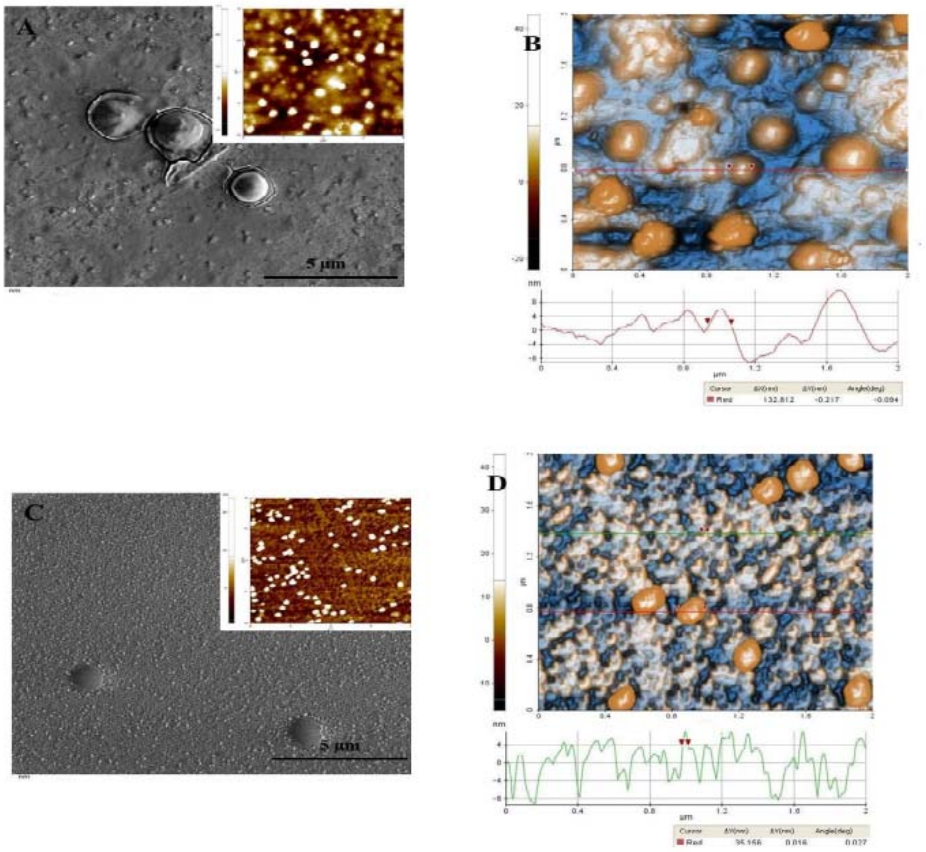

Fig.17. *Surface morphology for $Ge_{27}As_{13}S_{50}Te_{10}$ before and after the quality standard tests by AFM and SEM.*

The geometrical disorder of the chalcogenides forms a short range of localized energy band edges. Usually, two narrow bands are formed, proportional to the concentration of Ge (Fig. 18). The localized states originate due to lack of long-range interaction between atoms.

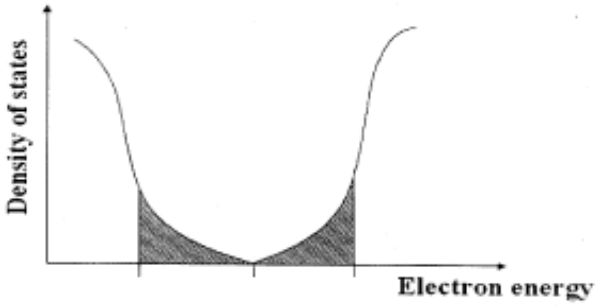

Fig.18. Energy band model for chalcogenides.

AKNOWLEDGEMENT

I am deeply grateful to Mariuca Gartner, Mihai Anastasescu, Hermine Stroescu, Madalina Nicolescu, Mihai Stoica and the whole team Anna Szekeres, Fabian Margit for guidance and persistent help in writing of this review paper.

REFERENCES

1. WOOD, R.W., *On a remarkable case of uneven distribution of light in a diffraction grating spectrum* Phil. Mag., 3, 607, 1902.
2. MEIER, W., *Eisenaufdampfschichten mit reproduzierbaren optischen Konstanten.* Ann. Phys., 31, 1017, 1910.
3. POPESCU, M.A., *Non-Crystalline Calcogenides*, Chap 4, Kluwer Academic Publisher, Dordrecht, 2000.
4. POPESCU, M., *Physics and Applications of Disordered Materials*, Ed. INOE, Bucharest, 2002.
5. GURINDER KAUR AHLUWALIA (Ed.), *Applications of calcogenide*s: *S, Se and Te,* 2014.
6. KOLOMIETS, B. T., *Vitreous Semiconductors* (I), Physica status solidi (b), 7 (2), 359–372, 1964.
7. KOLOMIETS, B. T., V*itreous Semiconductors* (II), Physica status solidi (b), 7 (3), 713–731, 1964.
8. REZNIK, N., Komljenovic, P.T., Germann, S., Rowlands, J.A., *Digital radiography using amorphous selenium: Photoconductivity activated switch (PAS) readout system*, Med. Phys., 35, 1039-1050, 2008.
9. OHTA, T., *Photo-Induced Metastability in Amorphous Semiconductors*, (Ed.) A.V. Kolobov, Wiley-VCH GmbH & Co. KgaA, Weinheim, 2006.
10. MUSGRAVES, J.D., DANTO, S., RICHARDSON, K., *Chalcogenide Glass Thin Film and Fiber Structures for Chemical and Biological Sensing*, 1-37, ebook, Chapter X, Ed. Univ.of Delaware, 2012**.**
11. TEJASWINI. M. L., VARUN. KUMAR A., Proc. of Int. Conf. on Current Trends in Eng., Science and Technology, ICCTEST 1014-1016, 2017.
12. Military Specification. Coating, Single or Multilayer, Interference: Durability Requirements; MIL-C-48497 Revision A, pp. 1–14, 1980.
13. ZAKERY, A., Journal of Optoelectronics and Advanced Materials, Vol. 7, No. 3, p.1143 - 1155 June 2005.
14. WELLS, A.F., *Structural Inorganic Chemistry*, Oxford: Clarendon Press, pg. 1-17 vol I 1984
15. VAUGHAN, D. J.; CRAIG, J. R. *Mineral Chemistry of Metal Sulfides*, pg. 20-25, Cambridge University Press, 1978.
16. WELLS, A.F., *Structural Inorganic Chemistry*, Oxford: Clarendon Press pg.1-35 vol II, 2012.
17. VAUGHAN, D. J., American Mineralogist, Vol 70, pg. 1036-1043, 1988.
18. PAUL H. RIBBE, *Sulfide Mineralogy*, Volume 1, pg. 1-12, Ed. Mineralogical Society of America, 1974.
19. FREUND, L.B., SURESH, S., *Thin film materials, stress, defect formation and surface evolution*, pg. 7-14, Cambridge Press, 2001.
20. DONALD L. SMITH, *Thin film- deposition Principles & Practice,* Chap 4, 167-175, Ed. McGraw-Hill New York, 2000.
21. DUMBRAVA, A., BADEA, C., PRODAN, G., CIUPINA, V., *Chalcogenide*, Lett., 7 (2) 111-118, 2010.
22. LUNGU, C.P. *et al*., Journ. of Optoel and Adv. Mat., 8(1), 74 – 77, 2006.
23. VLADOIU, R, *et al.*, *Chalcogenide*, Rom. Journ. Phys., 51(1-2), 2006.
24. POPA GHEORGHE, *Aplicaţii tehnologice ale plasmei,* pg. 10-48, Editura Iasi 1992.
25. AXLVITCH, Al., YOSII ROSENWAKS, GADY GOLAN, *Atomic layer deposition of noble metals: Exploration of the low limit of the deposition temperature,* J. Matter. Res., 19, 3353-3358, 2004.
26. MOSHINSKY, L., *Epoxy resins and dardeners*, ebook, Arcady-Press, 345-477, 1995.

27. MAIRAJ, A.K., *Optical Wavguide and Lasers in Improved Gallium Lanthanum Sulphide Glass*, PhD thesis, University of Southampton, Southampton, UK, 2003.
28. DULGHERU (NEDELCU), N., *Correlation of optical and morph-structural properties in chalcogenide compounds with applications in optoelectronics*, PhD thesis Romanian Academy "Ilie Murgulescu" Institute of Physical Chemistry, 2019.
29. DULGHERU (NEDELCU), N., ANASTASESCU, M., NICOLESCU, M., STOICA, M., GARTNER, M., PAMUKCHIEVA, V., SZEKERES, A., TODOROVA, K., *Surface topography and optical properties of Ge-Sb(As)-S-Te thin films by atomic-force microscopy and variable angle spectroscopic ellipsometry*, Journal of Physics: Conference Series, 356, 012019, 2012.
30. FABIAN, M., DULGHERU, N., ANTONOVA, K., SZEKERES, A., GARTNER, M., *Investigation of the Atomic Structure of Ge-Sb-Se Chalcogenide Glasses*, Advances in Condensed Matter Physics, vol. 2018, Article ID 7158079.
31. DULGHERU, N., M. GARTNER, M. ANASTASESCU, M. STOICA, M. NICOLESCU, H. STROESCU, I. ATKINSON, V. BRATAN, I. STANCULESCU, A. SZEKERES, P. TERZIYSKA, M. FABIAN, *Influence of compositional variation on the optical and morphological properties of GeSeSe films for optoelectronics application*, Infrared Physics and Technology 93, 260–270 2018.
32. NEERAJ MEHTA, *Applications of chalcogenide glasses in electronics and optoelectronics: A review, Journal of scientific and industrial research,* Journal of Scientific & Industrial Research, Vol. 65, 777-786, 2006.

Received August 11, 2019